Energy Conversion and Management 249 (2021) 114843

Contents lists available at ScienceDirect

Energy Conversion and Management

journal homepage: www.elsevier.com/locate/enconman

Cascaded dual-loop organic Rankine cycle with alkanes and low global warming potential refrigerants as working fluids

Wameedh Khider Abbas Abbas [a], Jadran Vrabec [b,*]

[a] Thermodynamics and Energy Technology, University of Paderborn, Warburger Straße 100, 33098 Paderborn, Germany
[b] Thermodynamics and Process Engineering, Technical University of Berlin, Ernst-Reuter-Platz 1, 10587 Berlin, Germany

ARTICLE INFO

Keyword:
Cascaded dual-loop ORC
Low GWP refrigerants
Thermal efficiency
Critical temperature of working fluids

ABSTRACT

A cascaded dual-loop organic Rankine cycle (CD-ORC) consisting of a high-temperature ORC (HT-ORC) and a low-temperature ORC (LT-ORC) with a shared heat exchanger is studied. Thermal efficiency is investigated as a key indicator for system performance over a wide range of heat source temperature ranging from 170 °C to 330 °C. The relation between the thermal efficiency and the critical temperature of the working fluids is explored. For this purpose, six alkanes and 31 refrigerants with a low GWP (≤150) are considered as working fluids in the HT-ORC and the LT-ORC, respectively. Cyclohexane and cyclopentane are found to be suitable for the HT-ORC with a maximum thermal efficiency of 19.13% and 18.03%. The thermal efficiency of both loops is highly affected by the working fluids since it increases with the critical temperature. As a whole, the CD-ORC may achieve a total thermal efficiency of 25.24%, 24.88% and 24.60% when using the working fluid combinations cyclohexane-R1366mzz(Z), cyclohexane-R1233zd(E) or cyclohexane-butane. This indicates that low GWP refrigerants are well-suited for LT-ORC. Compared to regular ORC, CD-ORC systems may achieve a thermal efficiency that is better by around a quarter.

1. Introduction

The rise in population as well as urban and technology development was accompanied by a significantly increased demand for energy, which is met by fossil fuels as the primary energy source due to their availability and low cost. However, studies have analyzed the risks of using fossil fuels and their derivatives which entail extensive pollution and threaten environmental disasters in the future [1]. Pollution and increased carbon dioxide emissions were accompanied by climate change and unprecedented weather events. The IPCC reported on August 9, 2021 that the world will reach 1.5 °C of warming within the next twenty years. There is thus a growing need to find alternative fuels, clean power sources with less harmful emissions and impact on the environment [2,3].

A large body of literature has grown around the organic Rankine cycle (ORC) as a technology to generate power from low and medium temperature heat sources. The ORC is a sustainable technology for power generation because it can utilize heat from geothermal [4], solar [5], combined heat and power [6], biomass [7], waste heat from industrial processes [8,9] or other sources [10].

Many studies have investigated different ORC architectures to enhance system performance. It was shown that multi-loop ORC theoretically can achieve a better thermal efficiency and net power output than regular ORC systems. Moreover, they have the capacity to concurrently recover heat from different sources [11–18]. Multi-loop ORC consist of several ORC loops, where each loop operates under different conditions (temperature, pressure and mass flow rate). Generally, dual-loop ORC consist of a high-temperature loop (HT-ORC) and a low-temperature loop (LT-ORC). The HT-ORC (topping ORC) is driven by the main heat source, while the LT-ORC loop (bottoming ORC) employs residual heat from the HT-ORC and/or is driven by a secondary heat source. A dual-loop ORC may allow for a better temperature profile matching between the heat source and the working fluid in the power generating cycle, which improves thermal efficiency. The disadvantage of multi-loop systems is their higher cost since they require more components than regular ORC. Such systems are also characterized by more complexity in terms of devices, sensors and operational parameters that need to be orchestrated [19].

Ayachi et al. [20] made an exergetic optimization to examine regular and dual-loop ORC performance for heat source temperatures between 150 °C and 165 °C. The authors considered three low GWP refrigerants, i.e. R1234yf, butane and isobutene, and reported that the critical temperature of the working fluid is closely related to exergy efficiency.

* Corresponding author.
E-mail address: vrabec@tu-berlin.de (J. Vrabec).

https://doi.org/10.1016/j.enconman.2021.114843
Received 31 July 2021; Accepted 3 October 2021
Available online 21 October 2021

Nomenclature

C1	HT-ORC condenser [−]
C2	LT-ORC condenser [−]
HE1	HT-ORC heat exchanger [−]
HE2	LT-ORC heat exchanger [−]
GWP	Global warming potential [−]
G1	HT-ORC generator [−]
G2	LT-ORC generator [−]
LNG	Liquefied natural gas [−]
M0	Heating cycle pump [−]
M1	HT-ORC pump [−]
M2	LT-ORC pump [−]
M3	Cooling cycle pump [−]
c_p	Specific isobaric heat capacity [kJ/(kg K)]
$\dot{E}_{in}$	Exergy flow input [kW]
h	Specific enthalpy [kJ/kg]
$\dot{m}_{HC}$	Mass flow rate in heating cycle [kg/s]
$\dot{m}_{HT}$	Mass flow rate in HT-ORC [kg/s]
$\dot{m}_{LT}$	Mass flow rate in LT-ORC [kg/s]
M	Molar mass [g/mol]
p_c	Critical pressure [bar]
p_e	Evaporation pressure [bar]
$\dot{Q}$	Heat flow [kW]
s	Specific entropy [kJ/(kg K)]
T_c	Critical temperature [°C]
$\dot{W}_{net}$	Net power output [kW]
$\dot{W}_P$	Pump power [kW]
$\dot{W}_T$	Turbine power output [kW]
$\eta_{ex,HT}$	Exergy efficiency of HT-ORC [%]
η_t	Turbine efficiency [%]
η_{th}	Thermal efficiency [%]

Kosmadakis et al. [21] tested 33 refrigerants to select a suitable working fluid for the HT cycle of a dual-loop ORC, where the operating temperature is between 130 °C and 140 °C. They discussed the performance of selected refrigerants together with their environmental issues and found that low GWP refrigerants may allow for good power output and thermal efficiency.

Preissinger et al. [22] studied a dual-loop ORC system driven by a wood pellet heater and considered 35 working fluids to examine system performance. The authors presented a relationship between the system performance and the thermophysical properties (critical temperature, critical pressure and molar mass) of the working fluids. They reported that the overall thermal efficiency is affected more by the LT-ORC working fluid than by the HT-ORC working fluid.

A study of a dual-loop ORC for waste heat recovery from a catalytic membrane reactor with hydrocarbons and low GWP refrigerants as working fluids has been presented by Fouad [23]. The author showed that the highest thermal efficiency was achieved with heptane as a working fluid in the HT-ORC. He found that R1234ze(Z) is a suitable alternative for R245fa and reported a maximum overall thermal efficiency of 13.39%.

Shu et al. [24] proposed a dual-loop ORC and analyzed the impact of the working fluid and other parameters on system performance. The proposed system consists of a HT-ORC to recover waste heat from exhaust gas and a LT-ORC to recover the residual heat from the HT-ORC and engine coolant. The authors selected six low GWP refrigerants for the LT-ORC and reported that the highest net power output was achieved with R1234yf. On the other hand, the maximum thermal efficiency was obtained with butane.

Wang et al. [25] investigated sub- and supercritical dual-loop ORC to recover waste heat from internal combustion engines. They utilized four pairs of working fluids, including two low GWP refrigerants, i.e. R1234yf and R1233zd(E). The authors showed that these are the most appropriate for dual-loop ORC among the considered working fluids.

Emadi et al. [26] studied working fluid selection for a dual-loop ORC, where the HT-ORC recovers heat from a solid-oxide fuel cell, while the LT-ORC was driven by LNG cryogenic energy. They considered 17 low GWP refrigerants and hydrocarbons to investigate performance in terms of exergy efficiency and turbine power output. It was found that maximum exergy efficiency and power output are achieved with a combination of hydrocarbons.

Xia et al. [27] made a theoretical investigation on working fluids for dual-loop ORC by employing their normal boiling point as a selection criterion. The authors studied 27 candidate pairs to choose combinations for HT-ORC and LT-ORC to maximize performance. They found that the optimal combination is cyclohexane-butane for the HT-ORC and LT-ORC, respectively.

Xue et al. [28] analyzed a dual-loop ORC layout to recover waste heat from LNG cryogenic energy and a gas-steam combined cycle power plant by taking two refrigerants as working fluids in the HT-ORC and LT-ORC. They studied the influence of operational conditions, such as mass flow rate and turbine inlet pressure, on performance. It was found that the maximum thermal efficiency was 25.64%.

The exergetic optimization of dual-loop ORC for waste heat recovery was studied by Braimaikis et al. [19]. They employed seven low GWP working fluids (three refrigerants and four hydrocarbons) to investigate the exergy efficiency for a heat source temperature between 100 °C and 300 °C. The authors compared dual-loop ORC with regular ORC and reported that the exergy efficiency of dual-loop ORC improves by up to a quarter when using cyclopentane and butane in the HT-ORC and LT-ORC, respectively. They noted that the dual-loop ORC is appropriate when the difference between the critical temperature of the working fluids and the heat source temperature is small.

This literature overview outlines that the dual-loop ORC is a promising technology for power generation and efficient utilization of heat sources. It also demonstrates that low GWP refrigerants are advantageous working fluids for dual-loop ORC because of environmental and safety aspects. To improve dual-loop ORC technology, more studies are needed for further development, which was the goal of this work. It was attempted to fill some of the gaps with a simulative investigation of dual-loop ORC technology by looking at a wide range of heat source temperature. Despite many studies on refrigerants, there is a lack of work that examines low GWP ($\leq$150) working fluids, especially zeotropic and azeotropic refrigerant mixtures. Several studies have considered refrigerants in ORC systems, but most have focused on specific groups only.

This paper considers six alkanes and 31 low GWP refrigerants as working fluids in the HT-ORC and LT-ORC, respectively. The selection criteria were based solely on environmental considerations, where the selected working fluids have a GWP value of up to 150 and zero or negligible ODP. The first goal was to estimate performance in terms of thermal efficiency over a wide range of heat source temperature by employing EBSILON@Professional as simulation software, resting on the most accurate equations of state for the thermophysical properties. The second goal was to investigate the correlation between critical temperature of the working fluid and thermal efficiency. The efficiency of a dual-loop ORC system is discussed by comparing with that of a regular ORC.

2. Working fluids

The selection of working fluids is a fundamental factor for ORC system design and performance. Many publications have demonstrated their vital role [37]. In case of dual-loop ORC, the working fluids in the HT-ORC and LT-ORC must match with each other and with the heat transfer fluid in the heating cycle. Several considerations have to be taken into account in this selection to satisfy the relevant requirements, including environmental friendliness, thermophysical characteristics, specific heat, heat transfer properties, chemical stability, material capability, safety, availability in the market and cost [40,41]. A considerable amount of literature deals with the impact of thermophysical properties on ORC system performance, including its relationship with the boiling point [29,30], molar mass [31,32], Jacob number [33,34] and critical temperature [35,36]. Most investigations have focused on the relationship between the thermal efficiency and the critical temperature. Song et al. [35] reported that working fluids with a higher critical temperature may achieve a better thermal efficiency. Barse and Mann [38] as well as Aljundi [39] also reported a strong relation between thermal efficiency and critical temperature of the working fluids, which rise together.

Vivian et al. [42] proposed that the optimum difference between the heat source temperature and the critical temperature of the working fluid is 35 °C, while Zhai et al. [43] showed that this difference varies between 35 °C and 50 °C. Braimakis et al. [19] found that a small gap between heat source temperature and critical temperature of the working fluid is favorable.

In this study, the thermal efficiency was investigated by considering different working fluids over a wide range of heat source temperature. 37 working fluids were examined to analyze the impact of their critical temperature on the thermal efficiency of the HT-ORC and the LT-ORC separately as well as overall system performance. The critical temperature of the selected working fluids varies from 85.60 °C to 295.59 °C, while the critical pressure varies between 24.83 bar and 55.79 bar.

2.1. Heating cycle

As a source, electric heaters were assumed so that a suitable heat transfer fluid is needed to transfer heat efficiently from the heating cycle (HC) to the HT-ORC. Therminol 66 was selected for this purpose due to its capability to operate over a wide range of temperature up to 345 °C. Therminol 66 has a low vapor pressure, good thermal stability and is

Table 1
Properties of working fluids considered in this work.

Substance	IUPAC name/Composition*	T_c [°C]	p_c [bar]	M [g/mol]	ODP	GWP	Refs.
Alkanes							
Octane	Octane	295.59	24.836	114.23	0	~20	[40,83]
Cyclohexane	Cyclohexane	280.45	40.805	84.159	0	~20	[40,85]
Heptane	Heptane	267.05	27.357	100.2	0	~20	[40,83]
Cyclopentane	Cyclopentane	238.57	45.828	70.133	0	~20	[40,86]
Hexane	Hexane	234.67	30.441	86.175	0	~20	[40,83]
R601	Pentane	196.55	33.675	72.149	0	~20	[40,83]
HFO							
R1366mzz(Z)	(Z)-1,1,1,4,4,4-Hexaflouro-2-butene	171.35	29.03	164.06	0	9	[83,96]
R1233zd(E)	*trans*-1-chloro-3,3,3-trifluoro-1-propene	166.45	36.237	130.5	0	4.5	[87,96]
R1234ze(Z)	*cis*-1,3,3,3-Tetrafluoropropene	150.12	35.306	114.04	0	7	[89,96]
R1234ze(E)	*trans*-1,3,3,3-Tetrafluoropropene	109.26	36.349	114.04	0	7	[92,96]
R1243zf	3,3,3-Trifluoropropene	103.78	35.179	96.051	0	149	[83,96]
R1234yf	2,3,3,3-Tetrafluoroprop-1-ene	94.7	33.822	114.04	0	4	[95,96]
HC							
R600	Butane	151.98	37.96	58.122	0	4	[88,96]
R600a	Isobutane	134.66	36.29	58.122	0	3	[88,96]
RE170	Dimethyl ether	127.23	53.368	46.068	0	3	[90,96]
Cyclopropane	Cyclopropane	125.15	55.797	42.081	0	~20	[40,83]
R290	Propane	96.74	42.512	44.096	0	3	[94,96]
R1270	Propylene	91.061	45.55	42.08	0	2	[83,96]
HFC							
R152a	1,1-Difluoroethane	113.26	45.168	66.051	0	124	[91,96]
R161	Fluoroethane	102.1	50.46	48.06	0	12	[93,96]
HC mixtures							
R510	0.88 RE170, 0.12 R600a	125.67	51.186	47.244	0	3	[83,97]
R441A	0.031 R170, 0.548 R290, 0.06 R600a, 0.361 R600	118.47	44.928	48.305	0	0	[83,96]
R436B	0.52 R290, 0.48 R600a	117.43	42.509	49.873	0	20	[83,97]
R436A	0.56 R290, 0.44 R600a	115.89	42.728	49.334	0	20	[83,97]
R432A	0.8 R1270, 0.2 RE170	97.256	47.564	42.821	0	16	[83,97]
R511A	0.95 R290, 0.05 RE170	96.977	42.879	44.19	0	9	[83,96]
R433A	0.3 R1270, 0.7 R290	94.416	43.454	43.471	0	20	[83,97]
HC/HFC mixtures							
R435A	0.8 RE170, 0.2 R152a	123.07	51.919	49.035	0	27	[83,96]
R429A	0.6 RE170, 0.1 R152a, 0.3 R600a	121.95	47.297	50.762	0	14	[83,96]
R430A	0.76 R152a, 0.24 R600a	107.2	40.891	63.957	0	110	[83,96]
R431A	0.71 R290, 0.29 R152a	89.591	42.069	48.8	0	53	[83,96]
HFC/HFO mixtures							
R444A	0.12 R32, 0.05 R152a, 0.83 R1234ze(E)	106.36	44.728	96.696	0	150	[83,96]
R451A	0.898 R1234yf, 0.102 R134a	94.364	34.43	112.69	0	149	[83,96]
R457A	0.18 R32, 0.12 R152a, 0.7 R1234yf	90.046	43.08	87.605	0	139	[83,96]
R459B	0.21 R32, 0.69 R1234yf, 0.10 R1234ze(E)	87.468	43.606	91.208	0	145	[83,96]
R454C	0.215 R32, 0.785 R1234yf	85.669	43.188	90.776	0	148	[83,96]
R455A	0.03 CO2, 0.215 R32, 0.755 R1234yf	85.609	46.538	87.453	0	145	[83,96]

*The composition is given in terms of the mass fraction.

non-corrosive to metals utilized in the construction of heating systems [44]. It was selected and recommended as a heat transfer fluid in ORC systems for different heat sources [45–47]. Its properties are listed in Table S1 in the supplementary material.

2.2. High-temperature cycle

Six alkanes were considered as working fluids for the HT-ORC cycle. They comprise four linear alkanes (pentane, hexane, heptane and octane) and two cyclic alkanes (cyclopentane and cyclohexane). The shorter four alkanes (methane, ethane, propane and butane) are not preferred in HT-ORC due to their low critical temperature. In addition, the working fluids for the HT-ORC were selected to satisfy operational requirements, being suitable with the heat source temperature [13,48–52]. The selected alkanes have the desired properties for working fluids in HT-ORC: thermal stability, material compatibility, appropriate critical temperature and pressure, low toxicity, zero ODP and low GWP. Moreover, alkanes exhibit a good performance and high efficiency in HT-ORC systems [52,53]. The critical temperature of these working fluids varies from 196.55 °C to 295.59 °C, while the critical pressure varies between 24.83 bar and 45.82 bar. The properties of the considered HT-ORC working fluids are listed in Table 1.

2.3. Low-temperature cycle

Global warming and ozone depletion are among the biggest challenges that the world faces. Several conventions and protocols emerged, such as the Montreal Protocol [54], Kyoto Protocol [55] and European regulations [56], to protect the ozone layer by eliminating or reducing the production of substances that are responsible for its depletion. The Montreal Protocol deals with excluding ozone-depleting refrigerants that contain either chlorine or bromine. In general, refrigerants can be classified according to their molecular composition into classes.

- Chlorofluorocarbons (CFC)

CFC refrigerants contain chlorine, fluorine and carbon atoms, such as R11, R12, R113, R114 or R115. These refrigerants were widely used in different applications due to their safety and thermodynamic properties. According to the Montreal Protocol, CFC refrigerants were phased out due to their high ODP and GWP values [57,58].

- Hydrochlorofluorocarbons (HCFC)

HCFC refrigerants contain hydrogen, chlorine, fluorine and carbon atoms, such as R22 or R123. These refrigerants are classified as having a medium to high GWP value and were introduced as substitutes for CFC due to thermodynamic similarity, intermediate ODP and somewhat lower GWP values. The Montreal Protocol was revised to phase out R22 by 2020 and all HCFC by 2030 [58].

- Hydrofluorocarbons (HFC)

HFC are the third generation of fluorine-based refrigerants and were introduced as transitional substitutes for CFC and HCFC. These refrigerants are classified as having zero ODP, but a significant GWP and were selected as alternatives for HCFC and CFC. Examples are R152a, R134a or R32 [59].

- Hydrofluoroolefins (HFO)

HFO contain hydrogen, fluorine and carbon atoms and represent the fourth generation of fluorine-based refrigerants, such as R1234yf, R1336zz(Z) or R1234ze(E). They are classified as environmentally friendly due to zero ODP and low GWP values so that they are a suitable alternative to CFC, HCFC and HFC refrigerants [60]. HFO are mildly flammable, may release hazardous substances, have a high price and require additional safety requirements [100,101]. The thermodynamic performance of HFO as working fluids in ORC systems is not well known. There is thus a need to evaluate favorable conditions (inlet temperature and pressure) under which a high thermal efficiency of ORC systems can be achieved [102].

- Hydrocarbons (HC)

HC are natural refrigerants, such as propane, propylene, butane or isobutane. These refrigerants are characterized by zero ODP, minimal GWP and low cost. HC refrigerants were introduced as alternatives for all existing fluorocarbon refrigerants that will phase out in the coming years. In addition, they are used as components in safety mixture fluids for small equipment applications [61].

- Refrigerant mixtures

Refrigerant mixtures are produced by blending pure refrigerants. They were introduced to provide fluids with a suitable thermodynamic behavior and to reduce undesired properties. Refrigerant mixtures may exhibit a good temperature profile match with heat transfer fluids in heat exchangers [62] and can be classified into:

Zeotropic mixtures, known as R5xx, contain two or more refrigerants species that have a different boiling point. This mixture type is characterized by a gliding condensation and evaporation temperature for a given pressure [63].

Azeotropic mixtures, known as R4xx, condensate and evaporate at a constant temperature for a given pressure so that they behave as pure refrigerants during phase change [64].

The implementation of European regulations on the environment and climate eliminated refrigerants with a high GWP, which includes R245fa and R134a, that are often used as working fluids in ORC systems [80]. Consequently, demand arose for alternatives of these eliminated refrigerants, which should have similar thermodynamic properties, good performance under different operational conditions and be environmentally friendly. Several studies suggested substitutes, such as HFO refrigerants [65], hydrocarbons, ammonia or carbon dioxide. Furthermore, refrigerant mixtures with tuned properties were proposed [66].

Lee et al. [67] presented two low GWP refrigerants, i.e. R455A and R454C, as suitable alternatives. Other studies have recommended synthetic refrigerants (R152a, R444A and R445A) for many applications as substitutes for high GWP refrigerants [68–70]. Xue et al. [71] and Sethi et al. [72] discussed that R600a and R455A can be considered as suitable for various applications due to desirable thermodynamic properties and lower GWP. Eyerer et al. [73] and Yang et al. [74] presented R1233zd(E) as an attractive alternative for R245fa in ORC systems. In addition, Molés et al. [75] and Yang et al. [76] assessed ORC system performance by utilizing R1336mzz(Z), R1234yf and R1233zd(E) as working fluids and alternatives for R245fa and R134a. The authors showed that such ORC systems could yield a higher thermal efficiency. Longo et al. [77] made a comparative study and showed that R1233zd(E) and R1234ze(Z) may lead to a similar or higher thermal efficiency than R245fa. Moreover, Bianchi et al. [78] laid out that R1234yf and R1234ze(E) are suitable substitutes for R134a in ORC systems. Devecioğlu et al. [79] considered a HFO/HFC mixture that showed an excellent performance. However, most research has focused on a specific group of refrigerants only. There is still a lack of investigations on other low GWP refrigerants, especially refrigerant mixtures, as working fluids in dual-loop ORC systems.

In this study, 31 refrigerants were considered as working fluids for the LT-ORC. All of them have a low GWP ($\leq$150) and negligible ODP. These working fluids include six HFO (R1366mzz(Z), R1233zd(E), R1234ze(Z), R1234ze(E), R1234yf and R1243zf), six HC (R600a, R290, R600, RE170, cyclopropane and R1270), seven HC mixtures (R510A, R511A, R436A, R436B, R432A, R433A and R441A), four HC/HFC

mixtures (R429A, R430A, R431A and R435A), six HFC/HFO mixtures (R444A, R451A, R454C, R455A, R457A and R459B) and two HFC refrigerants (R152a and R161). Their critical temperature varies from 85.60 °C to 171.35 °C, while their critical pressure lies between 29.03 bar and 55.79 bar. The properties of the selected refrigerants are listed in Table1.

3. System description

The simulated system is based on an actual CD-ORC test rig, which is experimentally set up and tested at the University of Paderborn [81]. The present simulations consider the two main operational cycles, i.e. HT-ORC and LT-ORC. The heat source of the CD-ORC is given by electrical heaters because of their inherently simple regulation and control, together with less strict safety and hazard requirements. Furthermore, electrical heaters as a thermal equivalent are a source allowing for a wide range of temperature. Their maximum thermal power is 158 kW to supply the main cycles with the required heat. Both cycles consist of the four essential components, i.e. turbine, evaporator, condenser and pump. The simulation parameters and components were selected to be close to the actual CD-ORC test rig.

In the heating cycle (HC), the heat transfer fluid (Therminol 66) is heated up by the electrical heaters and transferred to the HT-ORC. The HT-ORC utilizes that heat directly, while the LT-ORC utilizes the residual heat from the HT-ORC. In the HT cycle, the low-pressure saturated working fluid liquid is compressed by the HT-ORC feed pump (M1) and then enters the evaporator (HE1) to be vaporized isobarically into a saturated or superheated state. The working fluid at high pressure and temperature is supplied to the turbine (HT-turbine) to generate mechanical power and then electrical power via the generator (G1). After expansion, the working fluid is still at a high temperature and the residual heat is used to drive the LT-ORC. The expanded working fluid enters the condenser (C1) to release its remaining residual heat in an isobaric process.

A similar thermodynamic process occurs in the LT-ORC. The working fluid absorbs the heat from the HT-ORC and evaporates in HE2. It expands across the turbine (LT-turbine) to yield mechanical power output. Subsequently, the working fluid releases residual heat in the second condenser (C2) and is converted into a saturated liquid. Finally, the working fluid is compressed by the LT-ORC pump (M2) to continue the thermodynamic cycle.

4. Thermodynamic analysis

Simulations were carried out with EBSILON@Professional [82] to investigate system performance under different operating conditions. Various assumptions were made to build the simulation setup of the CD-ORC system depicted in Fig. 1.

Process (1–2): In this process, the heat transfer fluid Therminol 66 enters the HE1 to heat up and carry thermal energy to the HT-ORC. The heat flow can be calculated by

$$\dot{Q}_{HC} = \dot{m}_{HC}.c_p.(T_2 - T_1) \quad (1)$$

where $\dot{Q}_{HC}$ is the heat flow of the HC cycle, $\dot{m}_{HC}$ the mass flow rate, c_p the isobaric heat capacity of Therminol 66 and T_1 and T_2 are its temperatures at the inlet and outlet of HE1, respectively. The heat flow in the HC cycle is equal to the heat flow driving the HT-ORC (3–4), leading to isobaric evaporation and superheating of the alkane in the HT-ORC. The heat flow absorbed by the alkane in the HT-ORC can be expressed as

$$\dot{Q}_{HT} = \dot{m}_{HT}.(h_4 - h_3) \quad (2)$$

where $\dot{m}_{HT}$ is the mass flow rate of the alkane in the HT-ORC, h_3 and h_4 are its enthalpies at the inlet and outlet of HE1.

Process (4–5) refers to the adiabatic expansion work of the HT-turbine. High pressure and temperature alkane enters and expands across the HT-turbine into a low pressure state. The HT-turbine power output is given by

$$\dot{W}_{T,HT} = \dot{m}_{HT}.(h_4 - h_5) \quad (3)$$

where h_4 and h_5 are the enthalpies at the inlet and outlet.

Process (6–7) refers to the isobaric condensation of the alkane in the HT-ORC, which releases residual heat in condenser C1 and can be calculated by

$$\dot{Q}_{C1} = \dot{m}_{HT}.(h_6 - h_7) \quad (4)$$

where h_6 and h_7 are the enthalpies at the inlet and outlet.

Process (7–3) is the compression with pump M1 that can be determined as

$$\dot{W}_{P,HT} = \dot{m}_{HT}.(h_3 - h_7) \quad (5)$$

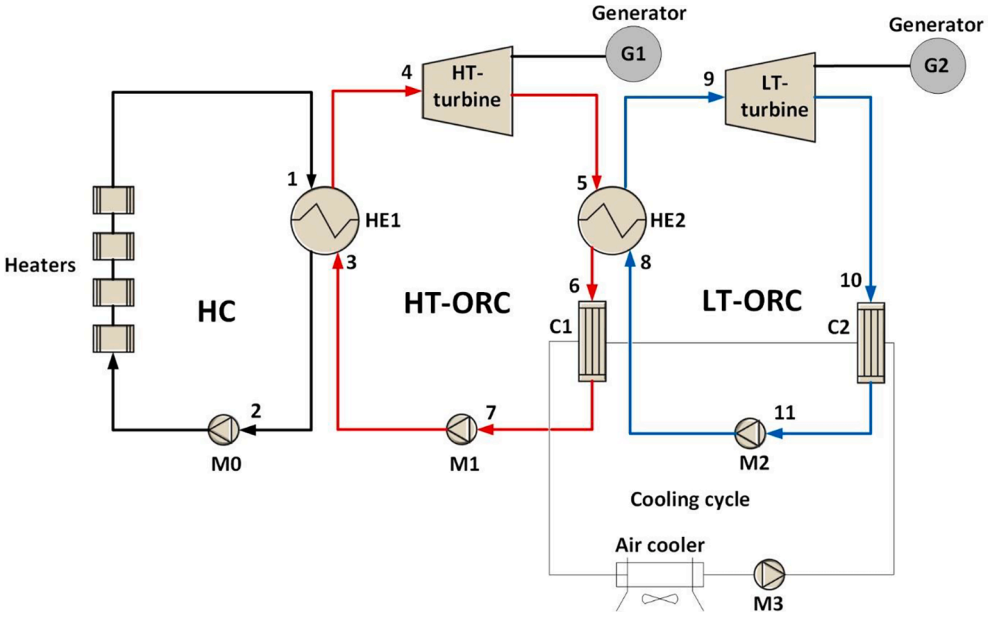

Fig. 1. Layout of the CD-ORC system investigated in the present work.

where h_7 and h_3 are the enthalpies at the inlet and outlet.

The thermal efficiency of the HT-ORC can be defined as the ratio of the net power output to the heat flow input to the HT-ORC

$$\eta_{th} = \frac{\dot{W}_{net,HT}}{\dot{Q}_{HT}} \tag{6}$$

where $\dot{W}_{net,HT} = \dot{W}_{T,HT} - \dot{W}_{P,HT}$.

Process (5–6): The heat flow from the HT-ORC is transferred to the LT-ORC via HE2 and is equal to that absorbed by the working fluid in the LT-ORC in process (8–9)

$$\dot{Q}_{LT} = \dot{m}_{LT}.(h_9 - h_8) \tag{7}$$

where $\dot{m}_{LT}$is the mass flow rate of the refrigerant in the LT-ORC, h_8 and h_9 are its enthalpies at the inlet and outlet.

Process (9–10) refers to the refrigerant expansion across the LT-ORC turbine and the power output is given by

$$\dot{W}_{T,LT} = \dot{m}_{LT}.(h_9 - h_{10}) \tag{8}$$

where h_9 and h_{10} are the enthalpies at the inlet and outlet.

Process (10–11) is the isobaric residual heat discharge of the refrigerant in the LT-ORC condenser C2

$$\dot{Q}_{C2} = \dot{m}_{LT}.(h_{10} - h_{11}) \tag{9}$$

where h_{10} and h_{11} are the enthalpies at the inlet and outlet.

Process (8–11): After condensation, the refrigerant is compressed adiabatically by the pump M2. The pump work in the LT-ORC is

$$\dot{W}_{P,LT} = \dot{m}_{LT}.(h_8 - h_{11}) \tag{10}$$

where h_{11} and h_8 are the enthalpies at the inlet and outlet.

The thermal efficiency of the LT-ORC can be defined as the ratio of the net power output to the heat flow input to the LT-ORC

$$\eta_{th} = \frac{\dot{W}_{net,LT}}{\dot{Q}_{LT}} \tag{11}$$

where $\dot{W}_{net,LT} = \dot{W}_{T,LT} - \dot{W}_{P,LT}$.

The total thermal efficiency of the CD-ORC is

$$\eta_{th,total} = \frac{\dot{W}_{net,total}}{\dot{Q}_{HC}} \tag{12}$$

where $\dot{W}_{net,total} = \dot{W}_{net,HT} + \dot{W}_{net,LT}$.

The exergy flow input can be calculated as

$$\dot{E}_{in} = \dot{m}_{HT}[(h_4 - h_3) - T_0(s_4 - s_3)] \tag{13}$$

where T_0 is the ambient temperature, h_3 and h_4 are working fluid enthalpies at the inlet and outlet of HE1, respectively, while s_3 and s_4 are the corresponding entropies.

The exergy efficiency of the HT-ORC can be calculated as

$$\eta_{ex,HT} = \frac{\dot{W}_{net,HT}}{\dot{E}_{in}} \tag{14}$$

Finally, the total exergy efficiency of the CD-ORC system can be calculated as

$$\eta_{ex,total} = \frac{\dot{W}_{net,total}}{\dot{E}_{in}} \tag{15}$$

5. Assumptions

The CD-ORC process was simulated with the software EBSILON@-Professional and the underlying thermophysical properties of the working fluids were supplied by REFPROP 10 [83] that rests on the most accurate equations of state as recommended by the National Institute of Science and Technology. The system was driven by heat from electrical heaters with a maximum heat flow of 158 kW. Evaporators and condensers of the CD-ORC system were assumed to be counter-current heat exchangers with a saturated or superheated outlet. It was operated under steady-state conditions in a steady flow process, neglecting potential and kinetic energy changes. Heat loss and pressure drop in pipelines and components as well as friction losses were neglected, except for turbine and pump efficiencies. The turbine inlet temperature was assumed to be lower than the critical temperature of the working fluid to avoid critical conditions. Isentropic efficiency of turbines and pumps in the HT-ORC and LT-ORC was set to 75% and the minimum pinch point temperature difference in evaporators and condensers was set to 5 °C. The minimum condensation temperatures were specified to be 50 °C and 35 °C in the HT-ORC and the LT-ORC, respectively. These assumptions and simulation parameters are listed in Table 2.

6. System validation

Due to the lack of work on CD-ORC systems (under the same operating conditions and the same working fluids), the present HT-ORC simulation was validated against literature data of a regular ORC system. The HT-ORC thermal efficiency was compared with results of Uusitalo et al. [84], where cyclohexane, cyclopentane, octane, heptane, hexane and pentane were considered as working fluids. To validate the present simulations, input parameters and conditions were the same as those in Ref. [84]: condensation temperature of 50 °C, η_t=0.75, no recuperator and a small degree of superheating were set for all working fluids in the HT-ORC and a maximum evaporation pressure ($p_e/p_c = 0.9$) was used to keep the working fluid below critical conditions. Moreover, the inlet state of the LT-ORC (heat flow and turbine inlet temperature) was compared with our previous experimental work using propane and butane as working fluids in the LT-ORC [81,98]. The thermal efficiency of butane was also compared with the study of Uusitalo et al. [84] at a turbine inlet temperature of 100 °C. The system behavior corresponded with the thermodynamic analysis of the thermal efficiency of the regular ORC system by using the same working fluids as in Refs. [52,53]. A comparison of the present work with these references is made in Table 3. Based on the good agreement with literature work, the present simulation model can be assumed to be validated.

7. Results and discussion

CD-ORC system performance in terms of thermal efficiency was simulated by adopting alkanes and low GWP refrigerants as working fluids. The first goal was to estimate the HT-ORC performance by employing cyclic and linear alkanes. The second goal was to simulate and analyze the entire CD-ORC and its overall system performance by

Table 2
Assumptions and operational conditions.

Parameter	value
Isentropic efficiency of turbines	75%
Mechanical efficiency of turbines	98%
Isentropic efficiency of pumps	75%
Mechanical efficiency of pumps	98%
Electric efficiency of pumps	85%
Efficiency of generators	90%
Power factor of generators	85%
Motor efficiency of pumps	85%
Minimum condensation temperature (HT-ORC)	50 °C
Minimum condensation temperature (LT-ORC)	35 °C
Minimum condensation pressure	1 bar
Mass flow rate of the HT-ORC	0.120–0.165 kg/s
Mass flow rate of the LT-ORC	0.05–0.10 kg/s
Minimum PPTD in evaporators	5 °C
Minimum PPTD in condensers	5 °C

Table 3
Comparison with the work by Uusitalo et al. [84].

Working fluid	Thermal efficiency [%]		Difference
	This work	Ref. [84]	
Cyclohexane	19.13	18.70	0.43
Cyclopentane	18.03	17.78	0.25
Octane	17.22	17.04	0.18
Heptane	16.23	16.52	0.29
Hexane	15.21	15.69	0.48
Pentane	13.92	14.08	0.16

utilizing low GWP refrigerants in the LT-ORC. A comparison between the regular ORC and the CD-ORC was made. This includes a study on the relationship between the critical temperature of the working fluid and the thermal efficiency as well as the effect of the HT-ORC on the LT-ORC. In addition, light is shed on the effectiveness of the CD-ORC for increasing the total thermal efficiency.

7.1. Thermal efficiency of the HT-ORC

A wide range of heat source temperature in increments of 10 °C was explored to study the thermal efficiency of the HT-ORC. Simulations were carried out by adopting cyclopentane, cyclohexane, pentane, hexane, heptane and octane as working fluids. The maximum applied heat source temperature was limited such that the HT-turbine inlet temperature was lower than the critical temperature of the given working fluid to avoid critical conditions. Consequently, the heat source temperature was in the range of 170–270 °C for cyclopentane, 170–320 °C for cyclohexane, 170–250 °C for pentane, 170–270 °C for hexane, 170–300 °C for heptane and 170–330 °C for octane.

Fig. 2 shows the thermal efficiency of the HT-ORC for this variation. As expected, an increasing trend of the thermal efficiency with heat source temperature was found for all working fluids. Simulation data indicate that cyclohexane has the most pronounced increase of thermal efficiency, while pentane has the lowest. The thermal efficiency increased from 11.53% to 19.13% for cyclohexane, from 11.28% to 18.03% for cyclopentane, from 9.52% to 17.22% for octane, from 8.83% to 16.22% for heptane, from 8.45% to 15.21% for hexane and from 7.95% to 13.92% for pentane. The main reason for that increasing trend is that the absorbed heat from the heating cycle and the net power output increase with rising heat source temperature. However, the net power output outweighs the increasing rate of the absorbed heat so that the thermal efficiency increases gradually with heat source temperature. Generally, a higher critical temperature is suitable for bringing the turbine inlet temperature to a high level, which may allow for an increase of the enthalpy difference across the turbine and leads to higher net power output and thermal efficiency. In addition, a higher critical temperature allows for a better use of the heat source. At a higher temperature, the heat flow carries a larger share of exergy, which is an indicator of the quality of energy.

The results show that the cyclic alkanes allow for a better thermal efficiency than the linear alkanes. Cyclic alkanes exhibit higher evaporation temperature levels, which leads to a suitable temperature match between heat source and working fluid to enhance the heat transfer between the heating cycle and the HT-ORC. Moreover, there is a direct correlation between thermal efficiency and critical temperature of the

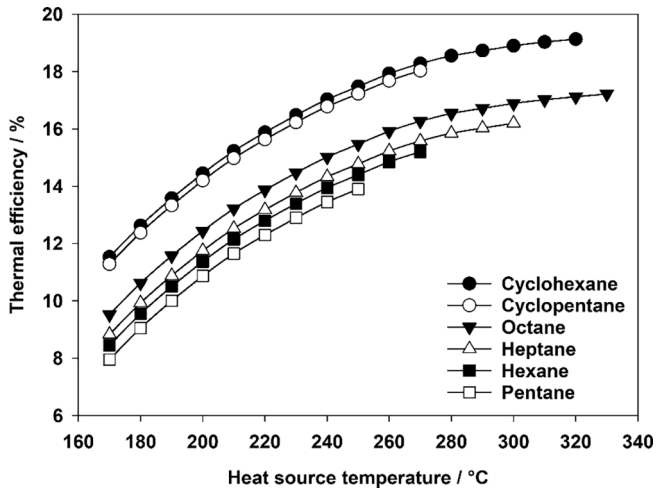

Fig. 2. Thermal efficiency of the HT-ORC as a function of heat source temperature for varying working fluids.

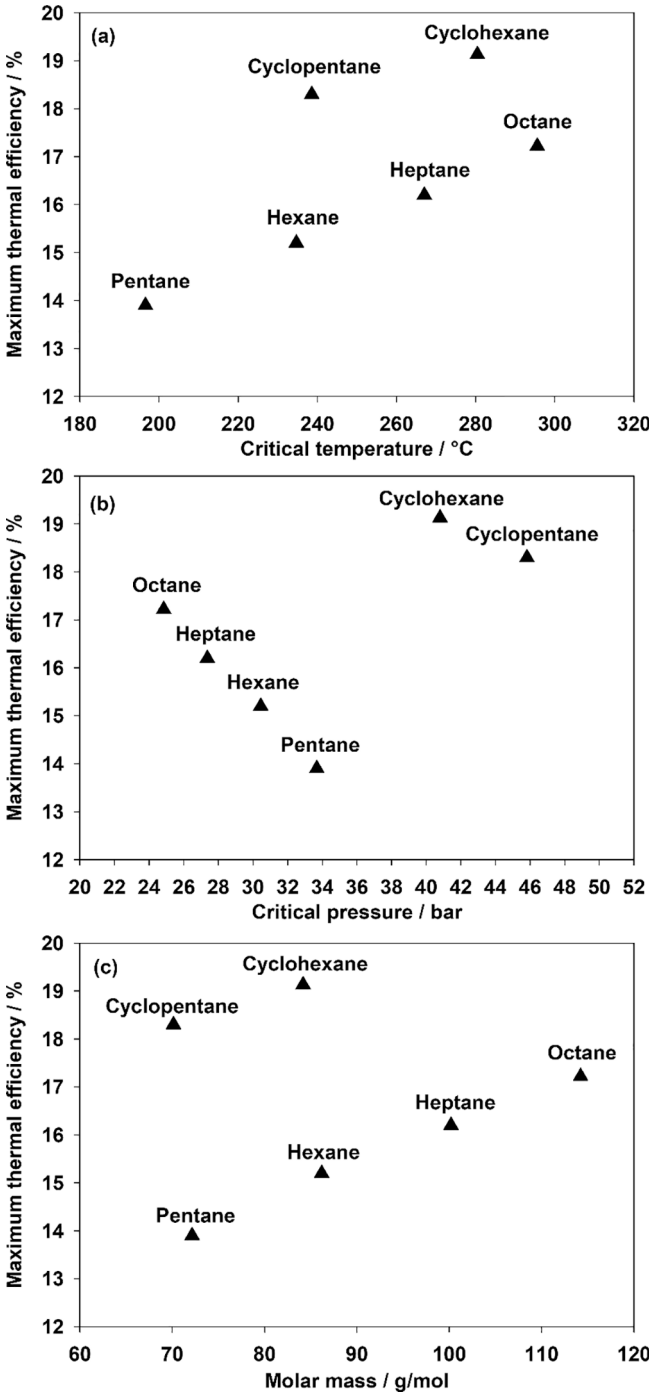

Fig. 3. Relation of the maximum thermal efficiency with (a) critical temperature, (b) critical pressure and (c) molar mass of the working fluid.

working fluid in each group. It can be seen that the thermal efficiency rises with the critical temperature of the working fluid. Fig. 3 depicts the relation between the thermophysical properties of working fluids and the maximum thermal efficiency of the HT-ORC. In each working fluid group (linear and cyclic alkanes), the thermal efficiency increases with rising critical temperature and molar mass. In contrast, it falls with increasing critical pressure in each working fluid group.

These results correspond to the findings of Shu et al. [52] and Liu et al. [53]. These authors investigated the thermal efficiency by employing cyclohexane, cyclopentane, octane, heptane, hexane and pentane as working fluids. They reported that the thermal efficiency of cyclohexane and cyclopentane is superior to that of linear alkanes. Uusitalo et al. [84] also showed that cyclic alkanes may achieve a higher thermal efficiency than linear alkanes.

7.2. Exergy flow analysis

Exergy indicates the quality of energy and defines the maximum achievable work during a process that brings the system into equilibrium with its environment [99]. An analysis was undertaken to determine the exergy flow input at the maximum applied heat source temperature, where each working fluid achieved its maximum thermal efficiency. Fig. 4(a) depicts the variation of exergy flow input with the maximum heat source temperature of the HT-ORC. The highest exergy flow input was 49.16 kW at a heat source temperature of 330 °C when using octane as working fluid, while the lowest exergy flow input was 36.92 kW at a heat source temperature of 250 °C when using pentane as a working fluid. In other words, the exergy flow input directly depends on the critical temperature of the working fluid. It also depends on the state of the system, the environment temperature and the temperature difference between the highest (the outlet of HE1) and lowest temperature (the inlet of HE1) as well as the mass flow rate of the working fluid. The inlet temperature of HE1 was constant for all working fluids, but the outlet state was limited by the critical temperature of the working fluid so that octane was capable to absorb the highest exergy flow input.

Fig. 4(b) depicts the variation of exergy efficiency of the HT-ORC at the maximum heat source temperature, where each working fluid achieved its maximum thermal efficiency. The highest exergy efficiency was 43.02% at a heat source temperature of 320 °C when using cyclohexane as a working fluid, while the lowest exergy efficiency was 31.58% at a heat source temperature of 250 °C when using pentane as a working fluid. In analogy to the thermal efficiency calculations, there is a direct correlation between exergetic efficiency and critical temperature of the working fluid in each group.

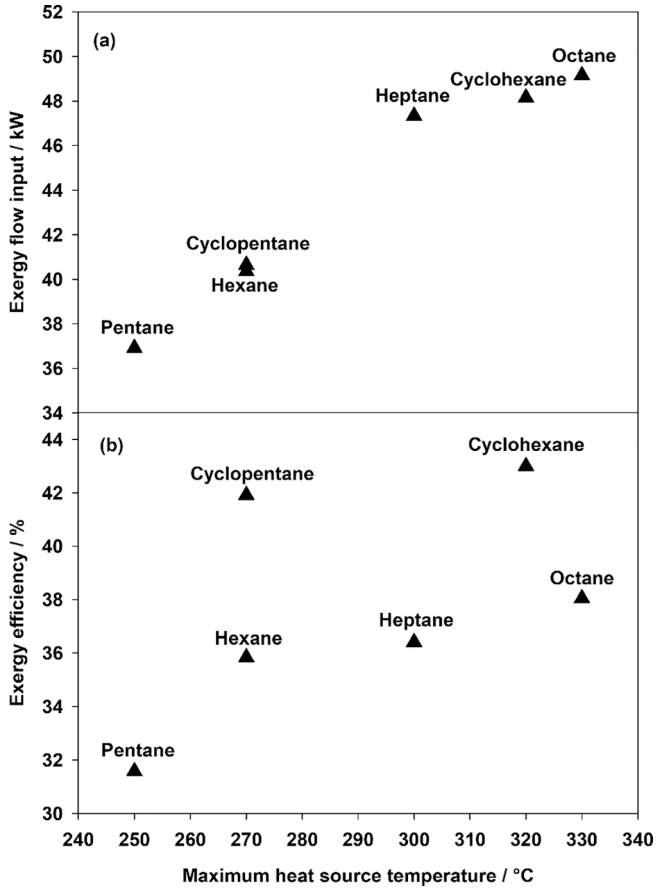

Fig. 4. Variation of (a) exergy flow input and (b) exergy efficiency at the maximum heat source temperature.

7.3. Thermal efficiency of the LT-ORC

The thermal efficiency of the LT-ORC was simulated for a wide heat source temperature range and only its maximum value is shown in Figs. 5(a)–8(a). Throughout, maximum thermal efficiency was achieved at the highest heat source temperature. The thermal efficiency was determined for all HT-ORC and LT-ORC working fluid combinations.

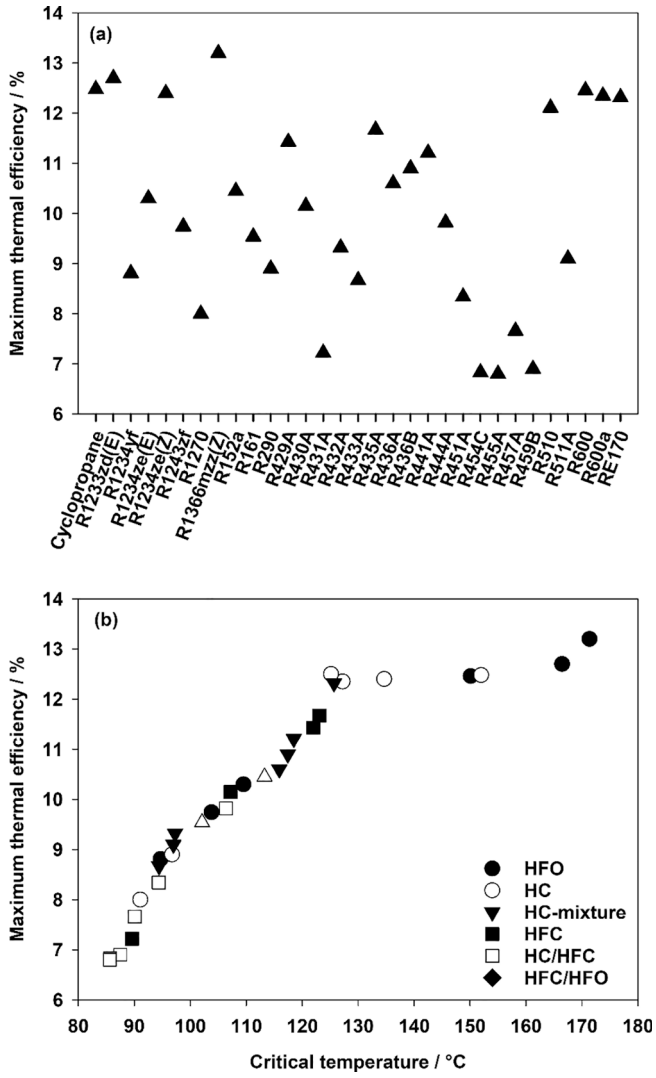

Fig. 5. (a) Variation of the LT-ORC maximum thermal efficiency by using cyclohexane as a working fluid in the HT-ORC and (b) relation between maximum thermal efficiency and critical temperature of the working fluid in the LT-ORC.

Figs. 5(b)–8(b) depict the variation of maximum thermal efficiency with critical temperature, where the LT-ORC working fluids are grouped.

Fig. 5(a) shows the maximum thermal efficiency of the LT-ORC when cyclohexane is used as a working fluid in the HT-ORC. The results represent data for a wide range of the heat source temperature from 170 °C to 330 °C. In general, it can be seen that there is a relation between the critical temperature of the working fluid and the efficiency, as shown in Fig. 5(b). Working fluids with a higher critical temperature in the range from 171.35 °C to 102.10 °C achieved a thermal efficiency from 13.20% to 9.32%, while refrigerants with a lower critical temperature in the range from 97.25 °C to 85.60 °C had a thermal efficiency from 9.54% to 6.81%. The LT-ORC has the highest thermal efficiency of 13.20% with R1366mzz(Z), followed by R1233zd(E) 12.70%, cyclopropane 12.50%, butane 12.48% and R1234ze(Z) 12.40%. The lowest thermal efficiency was 7.66%, 7.22%, 6.90%, 6.83% and 6.80% for R457A, R431A, R459B, R454C and R455A in the LT-ORC, respectively. Among the LT-ORC working fluids, the HC and HFO yield a higher thermal efficiency in the range from 13.20% to 8.02% compared to the other refrigerant groups.

Fig. 6(a) illustrates the LT-ORC thermal efficiency when using cyclopentane in the HT-ORC and varying refrigerants in the LT-ORC. The system was investigated for a heat source temperature range from 170 °C to 270 °C and the results also indicate that the thermal efficiency increases with the critical temperature for all refrigerants in the LT-ORC. The thermal efficiency of R1366mzz(Z), R1233zd(E), cyclopropane, butane and R1234ze(Z) is the highest. In contrast, lower thermal efficiency was achieved by R457A, R431A, R459B, R454C and R455A. Pure refrigerants, namely HFO, HC and HFC, achieved a thermal efficiency ranging from 7.45% to 11.86%, 6.77% to 11.58% and 8.32% to 8.85%, respectively. Moreover, a thermal efficiency from 7.12% to 10.65%, 6.11% to 9.87% and 5.70% to 8.65% was reached with HC, HC/HFC and HFC/HFO mixtures. Fig. 6(b) shows the increase of thermal efficiency with the critical temperature of the refrigerants.

Fig. 7(a) depicts the thermal efficiency of the LT-ORC by employing octane as a working fluid in the HT-ORC. The system was investigated for a heat source temperature range from 170 °C to 330 °C. The highest thermal efficiency was 13.40%, 13.22%, 13.20%, 13.11% and 13.08% for R1366mzz(Z), R1233zd(E), cyclopropane, butane and R1234ze(Z), respectively. In contrast, lower thermal efficiencies of 7.87%, 7.34%, 7.15%, 7.05% and 7.01% were found for R457A, R431A, R459B, R454C and R455A. Fig. 7(b) indicates that the pure refrigerant groups, namely HFO, HC and HFC, exhibit a thermal efficiency ranging from 9.11% to 13.40%, 8.10% to 13.11% and 9.75% to 10.78%. Thermal efficiency ranged from 9.03% to 12.22%, 7.34% to 11.98% and 7.01% to 10.02%

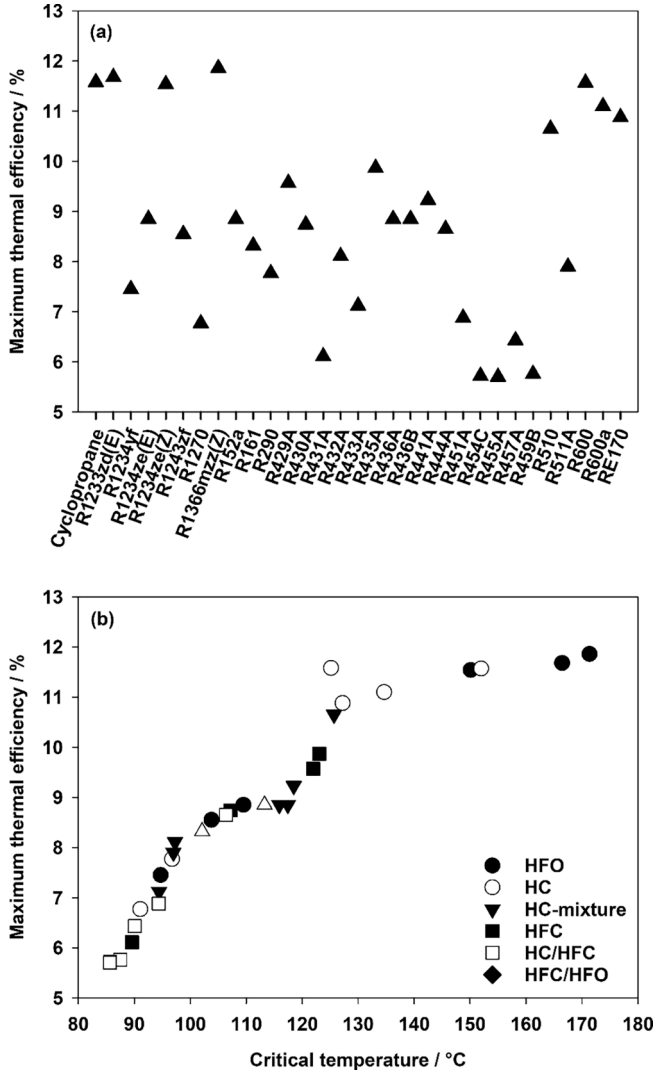

Fig. 6. (a) Variation of the LT-ORC maximum thermal efficiency by using cyclopentane as a working fluid in the HT-ORC and (b) relation between maximum thermal efficiency and critical temperature of the working fluid in the LT-ORC.

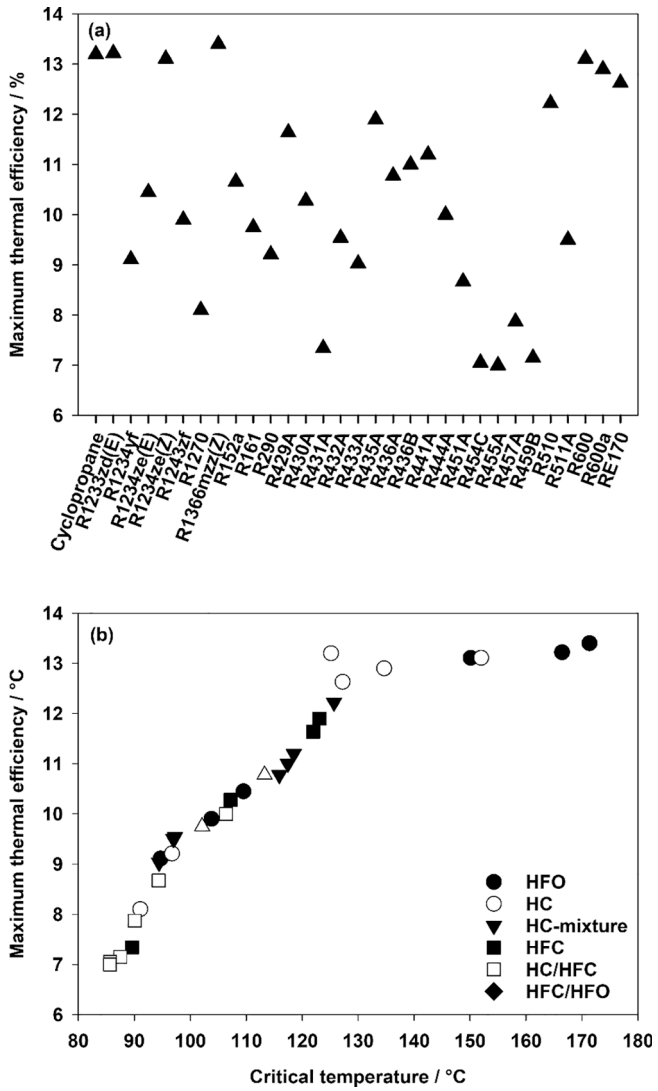

Fig. 7. (a) Variation of the LT-ORC maximum thermal efficiency by using octane as a working fluid in the HT-ORC and (b) relation between maximum thermal efficiency and critical temperature of the working fluid in the LT-ORC.

for HC, HC/HFC and HFC/HFO mixtures.

Fig. 8(a) illustrates the variation of the LT-ORC thermal efficiency when using heptane in the HT-ORC. The system was investigated for a heat source temperature range from 170 °C to 300 °C. The highest thermal efficiency was 12.20%, 12.00%, 11.98%, 11.95% and 11.90% by using R1366mzz(Z), R1233zd(E), cyclopropane, butane and R1234ze (Z), respectively. A thermal efficiency of 7.55%, 7.02%, 6.77%, 6.60% and 6.55% was found for R457A, R431A, R459B, R454C and R455A. Fig. 8(b) shows the increase of thermal efficiency with rising critical temperature of the refrigerants. The pure refrigerant groups, namely HFO, HC and HFC, exhibit a thermal efficiency ranging from 8.23% to 12.20%, 7.71% to 11.95% and 8.64% to 9.70%. Thermal efficiency ranged from 8.10% to 11.02%, 7.02% to 10.45% and 6.55% to 9.12% for HC, HC/HFC and HFC/HFO mixtures.

Hexane and pentane as working fluids in the HT-ORC lead to a further reduced thermal efficiency so that they are not described here in detail. The according results are depicted in Figs. S1 and S2 of the supplementary material.

The present data clearly indicate that pure fluids are preferred over refrigerant mixtures in any of the considered scenarios.

Fig. 9 summarizes the variation of the LT-ORC thermal efficiency for all working fluid combinations. It can be seen that the highest thermal efficiency of the LT-ORC was achieved with octane as a working fluid in the HT-ORC, while the lowest thermal efficiency was achieved with pentane as a working fluid in the HT-ORC. The figure demonstrates the effect of the working fluids' critical temperature on the thermal efficiency not only for the HT-ORC but also for the LT-ORC. For example, butane achieved a thermal efficiency of 13.11% when octane (with the highest critical temperature) was used as a working fluid in the HT-ORC. In comparison, butane achieved a thermal efficiency of only 8.80% when using pentane (with the lowest critical temperature) as a working fluid in the HT-ORC. Since the outlet of the HT-ORC turbine is the heat source of the LT-ORC, working fluids with a high critical temperature in the HT-ORC lead to an increase of the LT-ORC thermal efficiency.

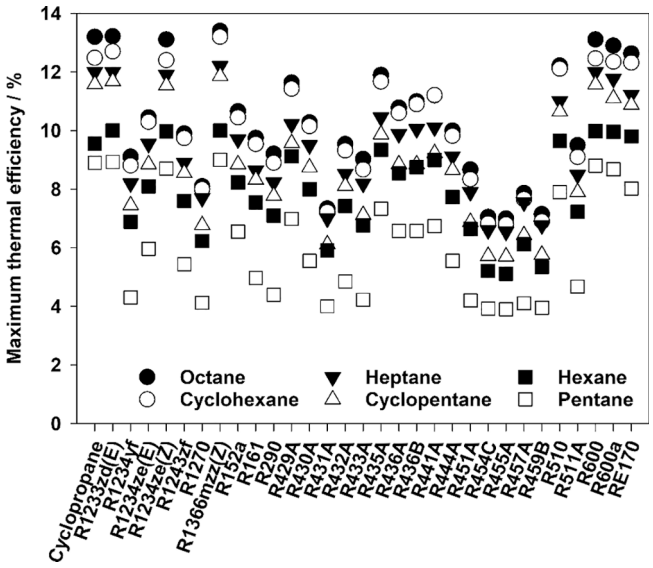

Fig. 9. Maximum thermal efficiency of the LT-ORC by utilizing cyclohexane, cyclopentane, octane, heptane, hexane and pentane as a working fluid in the HT-ORC.

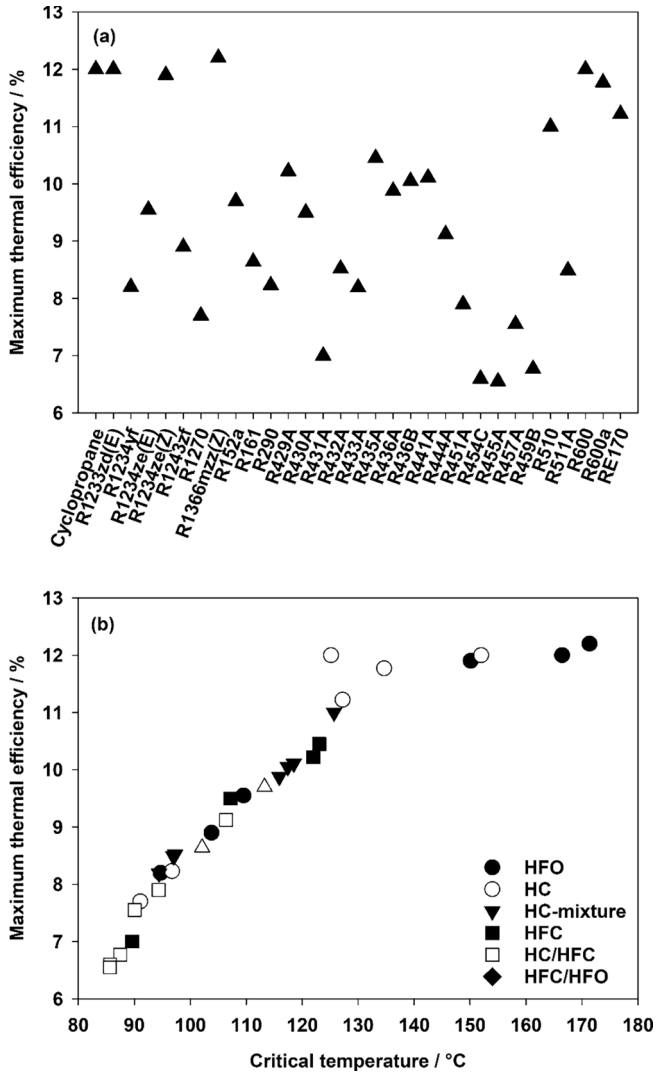

Fig. 8. (a) Variation of the LT-ORC maximum thermal efficiency by using heptane as a working fluid in the HT-ORC and (b) relation between maximum thermal efficiency and critical temperature of the working fluid in the LT-ORC.

It can be seen that the thermal efficiency of the LT-ORC is also highly affected by the critical temperature of the refrigerant. This can be explained by the fact that refrigerants with a high critical temperature allow for a higher turbine inlet temperature than refrigerants with a lower critical temperature. Moreover, a high critical temperature allows for a high evaporation temperature, which leads to an increase of thermal efficiency and an increase of the enthalpy difference across the turbine. Generally, a high critical temperature enhances the utilization of heat source temperature and is more suitable for temperature matching between the heat source and the working fluids. The effect of the critical temperature of alkanes acts not only on the HT-ORC, but on the LT-ORC as well.

Fig. 10 shows the total thermal efficiency of the CD-ORC for all working fluid combinations. The term (x-y) refers to x and y as working fluids in the HT-ORC and the LT-ORC, respectively. The results indicate that the highest total thermal efficiency of 25.24% was achieved by the combination (cyclohexane-R1366mzz(Z)) as working fluids in the CD-ORC system. In contrast, the lowest total thermal efficiency of 15.58% was obtained by employing the combination (pentane-R455A). A very high total thermal efficiency of 24.88%, 24.60%, 24.44% and 24.11% was also achieved by employing the combinations (cyclohexane-R1233zd(E)), (cyclohexane-butane), (cyclohexane-R1234ze(Z)) and (cyclohexane-isobutane), respectively.

7.4. Improvement of thermal efficiency

The total thermal efficiency of the CD-ORC was compared to that of a regular ORC under six conditions to analyze the percentage by which the thermal efficiency increased. This analysis is based on a comparison of

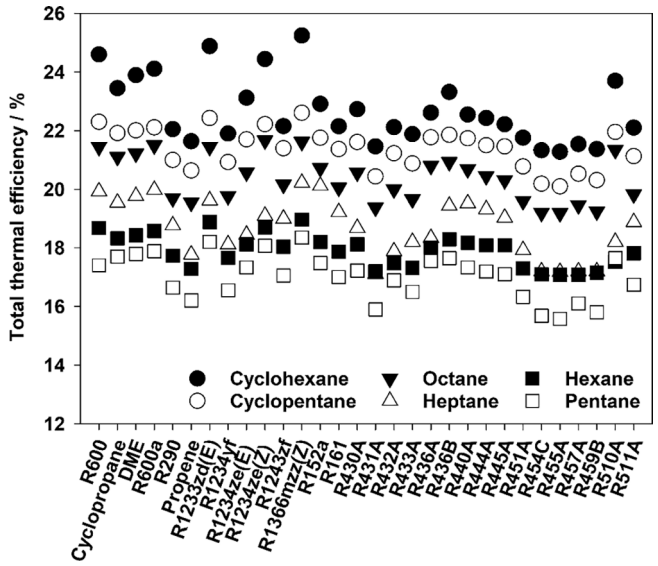

Fig. 10. Total thermal efficiency of the CD-ORC system.

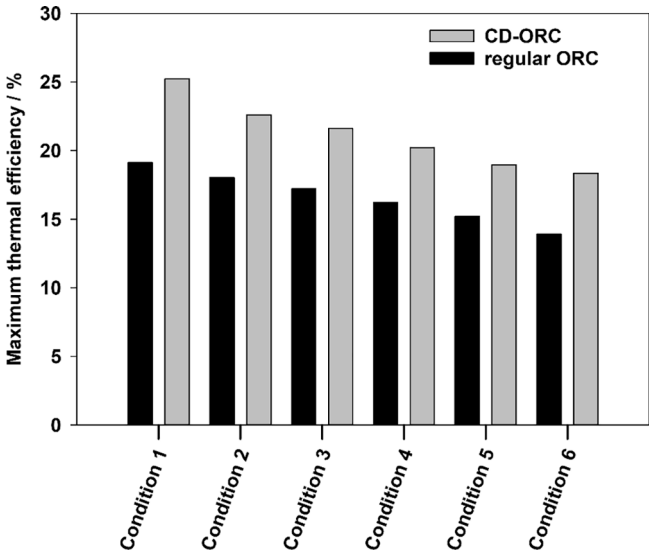

Fig. 11. Comparison of the thermal efficiency of CD-ORC and regular ORC under different operating conditions.

the highest thermal efficiency of the HT-ORC by adopting alkanes as a working fluid and the highest thermal efficiency of the CD-ORC system by adopting a combination of (alkane-R1366mzz(Z)). The combination (alkane-R1366mzz(Z)) was selected under all conditions because the CD-ORC always reached its highest total thermal efficiency by using R1366mzz(Z) in the LT-ORC. The combinations (cyclohexane-R1366mzz(Z)), (cyclopentane-R1366mzz(Z)), (octane-R1366mzz(Z)), (heptane-R1366mzz(Z)), (hexane-R1366mzz(Z)) and (pentane-R1366mzz(Z)) were used as working fluids under conditions (1) to (6) in the HT-ORC and LT-ORC of the CD-ORC system. The heat source temperature and the working fluids are listed in Table 4. Fig. 11 shows a comparison of the thermal efficiency of regular and CD-ORC under these conditions. The CD-ORC with the combination (cyclohexane-R1366mzz (Z) may enhance the thermal efficiency by a quarter, compared to the regular ORC (with cyclohexane as working fluid) at the maximum applied heat source temperature under condition (1). The comparison also shows the rise of the thermal efficiency under conditions (2) to (6), respectively. The results indicate that the thermal efficiency of the CD-ORC is higher than that of regular ORC, which is evidence of a more efficient utilization of the heat source. The addition of the LT-ORC in the CD-ORC led to more turbine power output and a higher thermal efficiency.

Table 4
Different conditions for comparison of the thermal efficiency of regular ORC and CD-ORC.

Condition (1)	
Heat source temperature	320 °C
Regular ORC working fluid	Cyclohexane
CD-ORC working fluids	Cyclohexane-R1366mzz(Z)
Condition (2)	
Heat source temperature	270 °C
Regular ORC working fluid	Cyclopentane
CD-ORC working fluids	Cyclopentane-R1366mzz(Z)
Condition (3)	
Heat source temperature	330 °C
Regular ORC working fluid	Octane
CD-ORC working fluids	Octane-R1366mzz(Z)
Condition (4)	
Heat source temperature	300 °C
Regular ORC working fluid	Heptane
CD-ORC working fluids	Heptane-R1366mzz(Z)
Condition (5)	
Heat source temperature	270 °C
Regular ORC working fluid	Hexane
CD-ORC working fluids	Hexane-R1366mzz(Z)
Condition (6)	
Heat source temperature	250 °C
Regular ORC working fluid	Pentane
CD-ORC working fluids	Pentane-R1366mzz(Z)

7.5. *Improvement of exergy efficiency*

This section focuses on the analysis of the total exergy efficiency that can be achieved with the CD-ORC system. The results indicate that the highest total exergy efficiency of 56.23% was achieved by the combination (cyclohexane-R1366mzz(Z)) as working fluids in the CD-ORC system. A very high total exergy efficiency of 54.85%, 54.23%, 53.54% and 53.14% was also achieved with the combinations (cyclohexane-R1233zd(E)), (cyclohexane-butane), (cyclohexane-R1234ze(Z)) and (cyclohexane-isobutane), respectively. By comparing the results of the total exergy efficiency of CD-ORC with that of the HT-ORC, the expected increase of the total exergy efficiency due to the increase of the net power output can be noticed. The results of exergy efficiency agree with the analysis of Braimakis et al. [19], who reported that the exergy efficiency may improve using a dual-loop ORC.

8. Conclusions

Alkanes and low GWP refrigerants were considered to investigate the thermal efficiency of the CD-ORC system. Simulations with EBSILON@Professional were carried out for a wide range of heat source temperature. The relation between the thermal efficiency and the critical temperature of the working fluids was analyzed. In the HT-ORC, the thermal efficiency is highly affected by the critical temperature, molecular mass and critical pressure. The results confirm that cyclic alkanes may achieve a higher thermal efficiency than linear alkanes. Thus, the thermal efficiency of alkanes rises with the critical temperature within the same group. Among the HT-ORC working fluids, cyclohexane provided the best thermal efficiency of 19.13%, while pentane achieved the worst thermal efficiency of 13.92%. The LT-ORC analysis with respect to the thermal efficiency was carried out by employing low GWP refrigerants as working fluids. Refrigerants with a high critical temperature are superior to other refrigerants. Relatively, R1366mzz(Z), R1233zde(E), cyclopropane, butane and R1234ze(Z) showed the highest thermal efficiency in the LT-ORC and refrigerant mixtures were found to

be less suitable. The CD-ORC system achieved a total thermal efficiency of 25.24%, 24.88%, 24.60%, 24.44% and 24.11% by utilizing the combinations (cyclohexane-R1366mzz(Z)), (cyclohexane-R1233zd(E)), (cyclohexane-butane), (cyclohexane-R1234ze(Z)) and (cyclohexane-isobutane), respectively. The CD-ORC system with a heat source temperature in the range from 170 °C to 330 °C exhibited a favorable performance when using refrigerants with a high critical temperature. Compared to the regular ORC, the CD-ORC system may lead to an increase of the thermal efficiency by up to a quarter. The results indicate that HFO refrigerants (namely R1366mzz(Z), R1233zd(E) and R1234ze (Z)) and HC refrigerants (namely butane, cyclopropane and isobutane) may be good alternatives for the refrigerants that are excluded by environmental regulations. Future work will include testing low GWP refrigerants as working fluids in CD-ORC systems practically, since our department has a CD-ORC test rig. Emphasis will also be placed on the simulation of environmentally friendly refrigerants under different conditions as working fluids in ORC as an alternative to excluded refrigerants.

Author contribution

Wameedh Khider Abbas Abbas has developed the simulation workflow, carried out the simulations, analyzed the results and wrote the manuscript. Jadran Vrabec initiated the project, supported this research and contributed to the manuscript's revision.

Declaration of Competing Interest

The authors declare that they have no known competing financial interests or personal relationships that could have appeared to influence the work reported in this paper.

Acknowledgements

We gratefully acknowledge the German Academic Exchange Service (DAAD) for financial support and the help provided by Dr. Gerhard Herres, University of Paderborn. The authors thank Dr. Antti Uusitalo, Lappeenranta University of Technology for providing data for the validation of the present simulation work.

Appendix A. Supplementary data

Supplementary data to this article can be found online at https://doi.org/10.1016/j.enconman.2021.114843.

References

[1] Prabhakaran SPS, Swaminathan G, Joshi VV. Thermogravimetric analysis of hazardous waste: Pet-coke, by kinetic models and Artificial neural network modelling. Fuel 2021;287:119470. https://doi.org/10.1016/j.fuel.2020.119470.
[2] Prabhakaran SPS, Swaminathan G, Joshi VV. Environmental Technology & Innovation Energy conservation – A novel approach of co-combustion of paint sludge and Australian lignite by principal component analysis, response surface methodology and artificial neural network modeling. Environ Technol Innov 2020;20:101061. https://doi.org/10.1016/j.eti.2020.101061.
[3] Jacob GA, Prabhakaran SPS, Swaminathan G, Joseyphus RJ. Thermal kinetic analysis of mustard biomass with equiatomic iron–nickel catalyst and its predictive modelling. Chemosphere 2022;286:131901. https://doi.org/10.1016/j.chemosphere.2021.131901.
[4] Liu X, Wang X, Zhang C. Sensitivity analysis of system parameters on the performance of the Organic Rankine Cycle system for binary-cycle geothermal power plants. Appl Therm Eng 2014;71:175–83. https://doi.org/10.1016/j.applthermaleng.2014.06.048.
[5] Wang M, Wang J, Zhao Y, Zhao P, Dai Y. Thermodynamic analysis and optimization of a solar-driven regenerative organic Rankine cycle (ORC) based on flat-plate solar collectors. Appl Therm Eng 2013;50:816–25. https://doi.org/10.1016/j.applthermaleng.2012.08.013.
[6] Farrokhi M, Noie SH, Akbarzadeh AA. Preliminary experimental investigation of a natural gas-fired ORC-based micro-CHP system for residential buildings. Appl Therm Eng 2014;69:221–9. https://doi.org/10.1016/j.applthermaleng.2013.11.060.
[7] Huang Y, McIlveen-Wright DR, Rezvani S, Huang MJ, Wang YD, Roskilly AP, et al. Comparative techno-economic analysis of biomass fuelled combined heat and power for commercial buildings. Appl Energy 2013;112:518–25. https://doi.org/10.1016/j.apenergy.2013.03.078.
[8] Dolz V, Novella R, García A, Sánchez J. HD Diesel engine equipped with a bottoming Rankine cycle as a waste heat recovery system. Part 1: Study and analysis of the waste heat energy. Appl Therm Eng 2012;36:269–78. https://doi.org/10.1016/j.applthermaleng.2011.10.025.
[9] Kwak DH, Binns M, Kim J-K. Integrated design and optimization of technologies for utilizing low grade heat in process industries. Appl Energy 2014;131:307–22. https://doi.org/10.1016/j.apenergy.2014.06.037.
[10] M.A. Al-Weshahi, A. Anderson, G. Tian, Organic Rankine Cycle recovering stage heat from MSF desalination distillate water, Appl. Energy 130 (2014) 738–747. doi.org/10.1016/j.apenergy.2014.02.038.
[11] Mehrpooya M, Ashouri M, Mohammadi A. Thermoeconomic analysis and optimization of a regenerative two-stage organic Rankine cycle coupled with liquefied natural gas and solar energy. Energy 2017;126:899–914. https://doi.org/10.1016/j.energy.2017.03.064.
[12] G. Shu, G. Yu, H. Tian, H. Wei, X. Liang, Z. Huang, Multi-approach evaluations of a cascade-Organic Rankine Cycle (C-ORC) system driven by diesel engine waste heat: Part A – Thermodynamic evaluations, Energy Convers. Manag. 108 (2016) 579–595. doi.org/10.1016/j.enconman.2015.10.084.
[13] Chen T, Zhuge W, Zhang Y, Zhang L. A novel cascade organic Rankine cycle (ORC) system for waste heat recovery of truck diesel engines. Energy Convers Manag 2017;138:210–23. https://doi.org/10.1016/j.enconman.2017.01.056.
[14] Yang F, Cho H, Zhang H, Zhang J. Thermoeconomic multi-objective optimization of a dual loop organic Rankine cycle (ORC) for CNG engine waste heat recovery. Appl Energy 2017;205:1100–18. https://doi.org/10.1016/j.apenergy.2017.08.127.
[15] Lim T, Choi Y, Hwang D. Optimal working fluids and economic estimation for both double stage organic Rankine cycle and added double stage organic Rankine cycle used for waste heat recovery from liquefied natural gas fueled ships. Energy Convers Manag 2021;242:114323. https://doi.org/10.1016/j.enconman.2021.114323.
[16] Yun E, Park H, Yoon SY, Kim KC. Dual parallel organic Rankine cycle (ORC) system for high efficiency waste heat recovery in marine application. J Mech Sci Technol 2015;29:2509–15. https://doi.org/10.1007/s12206-015-0548-5.
[17] Sung T, Kim KC. Thermodynamic analysis of a novel dual-loop organic Rankine cycle for engine waste heat and LNG cold. Appl Therm Eng 2016;100:1031–41. https://doi.org/10.1016/j.applthermaleng.2016.02.102.
[18] Ntavou E, Kosmadakis G, Manolakos D, Papadakis G, Papantonis D. Experimental testing of a small-scale two stage Organic Rankine Cycle engine operating at low temperature. Energy 2017;141:869–79. https://doi.org/10.1016/j.energy.2017.09.127.
[19] Braimakis K, Karellas S. Exergetic optimization of double stage Organic Rankine Cycle (ORC). Energy 2018;149:296–313. https://doi.org/10.1016/j.energy.2018.02.044.
[20] Ayachi F, Boulawz Ksayer E, Zoughaib A, Neveu P. ORC optimization for medium grade heat recovery. Energy 2014;68:47–56. https://doi.org/10.1016/j.energy.2014.01.066.
[21] Kosmadakis G, Manolakos D, Kyritsis S, Papadakis G. Comparative thermodynamic study of refrigerants to select the best for use in the high-temperature stage of a two-stage organic Rankine cycle for RO desalination. Desalinaion 2009;243:74–94. https://doi.org/10.1016/j.desal.2008.04.016.
[22] Preißinger M, Heberle F, Brüggemann D. Thermodynamic analysis of double-stage biomass fired Organic Rankine Cycle for micro-cogeneration. Int J Energy Res 2012;36:944–52. https://doi.org/10.1002/er.1952.
[23] Fouad WA. A combined heat, hydrogen and power tri-generation system based on the use of catalytic membrane reactors with a dual-loop organic Rankine cycle. Energy Convers Manag 2020;222:113255. https://doi.org/10.1016/j.enconman.2020.113255.
[24] Shu G, Liu L, Tian H, Wei H, Yu G. Parametric and working fluid analysis of a dual-loop organic Rankine cycle (DORC) used in engine waste heat recovery. Appl Energy 2014;113:1188–98. https://doi.org/10.1016/j.apenergy.2013.08.027.
[25] Wang E, Yu Z, Zhang H, Yang F. A regenerative supercritical-subcritical dual-loop organic Rankine cycle system for energy recovery from the waste heat of internal combustion engines. Appl Energy 2017;190:574–90. https://doi.org/10.1016/j.apenergy.2016.12.122.
[26] Emadi MA, Chitgar N, Oyewunmi OA, Markides CN. Working-fluid selection and thermoeconomic optimisation of a combined cycle cogeneration dual-loop organic Rankine cycle (ORC) system for solid oxide fuel cell (SOFC) waste-heat recovery. Appl Energy 2020;261:114384. https://doi.org/10.1016/j.apenergy.2019.114384.
[27] Xia XX, Wang ZQ, Zhou NJ, Hu YH, Zhang JP, Chen Y. Working fluid selection of dual-loop organic Rankine cycle using multi-objective optimization and improved grey relational analysis. Appl Therm Eng 2020;171:115028. https://doi.org/10.1016/j.applthermaleng.2020.115028.
[28] Xue X, Guo C, Du X, Yang L, Yang Y. Thermodynamic analysis and optimization of a two-stage organic Rankine cycle for liquefied natural gas cryogenic exergy recovery. Energy 2015;83:778–87. https://doi.org/10.1016/j.energy.2015.02.088.
[29] Kuo C, Hsu S, Chang K, Wang C. Analysis of a 50 kW organic Rankine cycle system. Energy 2011;36:5877–85. https://doi.org/10.1016/j.energy.2011.08.035.

[30] Mago PJ, Chamra LM, Somayaji C. Performance analysis of different working fluids for use in organic Rankine cycles. Proc Inst Mech Eng Part A J Power Energy 2007;221:255–64. https://doi.org/10.1243/09576509JPE372.
[31] Stijepovic MZ, Linke P, Papadopoulos AI, Grujic AS. On the role of working fluid properties in Organic Rankine Cycle performance. Appl Therm Eng 2012;36:406–13. https://doi.org/10.1016/j.applthermaleng.2011.10.057.
[32] Jung D, Park S, Min K. Selection of appropriate working fluids for Rankine cycles used for recovery of heat from exhaust gases of ICE in heavy-duty series hybrid electric vehicles. Appl Therm Eng 2015;81:338–45. https://doi.org/10.1016/j.applthermaleng.2015.02.002.
[33] Wang D, Ling X, Peng H, Liu L, Tao LL. Efficiency and optimal performance evaluation of organic Rankine cycle for low grade waste heat power generation. Energy 2013;50:343–52. https://doi.org/10.1016/j.energy.2012.11.010.
[34] He C, Liu C, Zhou M, Xie H, Xu X, Wu S, et al. A new selection principle of working fluids for subcritical organic Rankine cycle coupling with different heat sources. Energy 2014;68:283–91. https://doi.org/10.1016/j.energy.2014.02.050.
[35] Song C, Gu M, Miao Z, Liu C, Xu J. Effect of fluid dryness and critical temperature on trans-critical organic Rankine cycle. Energy 2019;174:97–109. https://doi.org/10.1016/j.energy.2019.02.171.
[36] Xu J, Yu C. Critical temperature criterion for selection of working fluids for subcritical pressure Organic Rankine cycles. Energy 2014;74:719–33. https://doi.org/10.1016/j.energy.2014.07.038.
[37] Lai NA, Wendland M, Fischer J. Working fluids for high-temperature organic Rankine cycles. Energy 2011;36:199–211. https://doi.org/10.1016/j.energy.2010.10.051.
[38] Barse KA, Mann MD. Maximizing ORC performance with optimal match of working fluid with system design. Appl Therm Eng 2016;100:11–9. https://doi.org/10.1016/j.applthermaleng.2016.01.167.
[39] Aljundi IH. Effect of dry hydrocarbons and critical point temperature on the efficiencies of organic Rankine cycle. Renew Energy 2011;36:1196–202. https://doi.org/10.1016/j.renene.2010.09.022.
[40] Zhai H, Shi L, An Q. Influence of working fluid properties on system performance and screen evaluation indicators for geothermal ORC (organic Rankine cycle) system. Energy 2014;74:2–11. https://doi.org/10.1016/j.energy.2013.12.030.
[41] Saleh B, Koglbauer G, Wendland M, Fischer J. Working fluids for low-temperature organic Rankine cycles. Energy 2007;32:1210–21. https://doi.org/10.1016/j.energy.2006.07.001.
[42] Vivian J, Manente G, Lazzaretto A. A general framework to select working fluid and configuration of ORCs for low-to-medium temperature heat sources. Appl Energy 2015;156:727–46. https://doi.org/10.1016/j.apenergy.2015.07.005.
[43] Zhai H, An Q, Shi L. Analysis of the quantitative correlation between the heat source temperature and the critical temperature of the optimal pure working fluid for subcritical organic Rankine cycles. Appl Therm Eng 2016;99:383–91. https://doi.org/10.1016/j.applthermaleng.2016.01.058.
[44] Eastman chemical company. Product data sheet Therminol 66. Website address: http://www.eastman.com/pages/products/therminol66.asp; accessed on 09th May 2021.
[45] Sterrer R, Schidler S, Schwandt O, Franz P, Hammerschmid A. Theoretical analysis of the combination of CSP with a biomass CHP-plant using ORC-technology in Central Europe. Energy Procedia 2014;49:1218–27. https://doi.org/10.1016/j.egypro.2014.03.131.
[46] Bianchi M, Branchini L, De Pascale A, Melino F, Orlandini V, Peretto A, et al. Techno-Economic Analysis of ORC in Gas Compression Stations Taking into Account Actual Operating Conditions. Energy Procedia 2017;129:543–50. https://doi.org/10.1016/j.egypro.2017.09.182.
[47] Tafone A, Borri E, Comodi G, Van Den Broek M, Romagnoli A. Preliminary assessment of waste heat recovery solution (ORC) to enhance the performance of Liquid Air Energy Storage system. Energy Procedia 2017;142:3609–16. https://doi.org/10.1016/j.egypro.2017.12.252.
[48] Song J, Song Y, Gu C. Thermodynamic analysis and performance optimization of an Organic Rankine Cycle (ORC) waste heat recovery system for marine diesel engines. Energy 2015;82:976–85. https://doi.org/10.1016/j.energy.2015.01.108.
[49] Tourkov K, Schaefer L. Performance evaluation of a PVT/ORC (photovoltaic thermal/organic Rankine cycle) system with optimization of the ORC and evaluation of several PV (photovoltaic) materials. Energy 2015;82:839–49. https://doi.org/10.1016/j.energy.2015.01.094.
[50] Siddiqi MA, Atakan B. Alkanes as fluids in Rankine cycles in comparison to water, benzene and toluene. Energy 2012;45:256–63. https://doi.org/10.1016/j.energy.2012.06.005.
[51] Tchanche BF, Papadakis G, Lambrinos G, Frangoudakis A. Fluid selection for a low-temperature solar organic Rankine cycle. Appl Therm Eng 2009;29:2468–76. https://doi.org/10.1016/j.applthermaleng.2008.12.025.
[52] Shu G, Li X, Tian H, Liang X, Wei H, Wang X. Alkanes as working fluids for high-temperature exhaust heat recovery of diesel engine using organic Rankine cycle. Appl Energy 2014;119:204–17. https://doi.org/10.1016/j.apenergy.2013.12.056.
[53] Liu P, Shu G, Tian H, Wang X, Yu Z. Alkanes based two-stage expansion with interheating Organic Rankine cycle for multi-waste heat recovery of truck diesel engine. Energy 2018;147:337–50. https://doi.org/10.1016/j.energy.2017.12.109.
[54] United Nations. Montreal Protocol on Substances That Deplete the Ozone Layer. Ozone Secretariat, New York, NY, USA: United Nations Environment Program; 1987.
[55] Occhipinti Z, Verona R. Kyoto Protocol (KP). In: Leal FW, Azul AM, Brandli L, Özuyar PG, Wall T, editors. Climate Action. Encyclopedia of the UN Sustainable Development Goals. Cham: Springer; 2020. https://doi.org/10.1007/978-3-319-95885-9_23.
[56] European Parliament. Regulation (EU) No 517/2017 of the European parliament and of the council of 16 april 2014 on fluorinated greenhouse gases and repealing regulation (EC) No 842/2006. Council of the European Union 2014.
[57] Kopko WL. Beyond CFCs: Extending the search for new refrigerants. Int J Refrig 1990;13:79–85. https://doi.org/10.1016/0140-7007(90)90005-H.
[58] Wang H, Zhao L, Cao R, Zeng W. Refrigerant alternative and optimization under the constraint of the greenhouse gas emissions reduction target. J Clean Prod 2021;296:126580. https://doi.org/10.1016/j.jclepro.2021.126580.
[59] Sánchez D, Cabello R, Llopis R, Arauzo I, Catalán-gil J, Torrella E. Energy performance evaluation of R1234yf, R1234ze(E), R600a, R290 and R152a as low-GWP R134a alternatives. Int J Refrig 2020;74:269–82. https://doi.org/10.1016/j.ijrefrig.2016.09.020.
[60] Albà CG, Vega LF, Llovell F. A consistent thermodynamic molecular model of n-hydrofluoroolefins and blends for refrigeration applications. Int J Refrig 2020;113:145–55. https://doi.org/10.1016/j.ijrefrig.2020.01.008.
[61] Mota-Babiloni A, Makhnatch P. Predictions of European refrigerants place on the market following F-gas regulation restrictions. Int J Refrig 2021;127:101–10. https://doi.org/10.1016/j.ijrefrig.2021.03.005.
[62] Xiao B, Chang H, He L, Zhao S, Shu S. Annual performance analysis of an air source heat pump water heater using a new eco-friendly refrigerant mixture as an alternative to R134a. Renew Energy 2020;147:2013–23. https://doi.org/10.1016/j.renene.2019.09.143.
[63] Dai B, Liu S, Li H, Sun Z, Song M, Yang Q, et al. Energetic performance of transcritical CO2 refrigeration cycles with mechanical subcooling using zeotropic mixture as refrigerant. Energy 2018;150:205–21. https://doi.org/10.1016/j.energy.2018.02.111.
[64] Morrison G, McLinden MO. Azeotropy in refrigerant mixtures. Int J Refrig 1993;16:129–38. https://doi.org/10.1016/0140-7007(93)90069-K.
[65] Vaitkus L, Dagilis V. Analysis of alternatives to high GWP refrigerants for eutectic refrigerating systems. Int J Refrig 2017;76:160–9. https://doi.org/10.1016/j.ijrefrig.2017.01.024.
[66] Li Z, Shen B, Gluesenkamp KR. Multi-objective optimization of low-GWP mixture composition and heat exchanger circuitry configuration for improved system performance and reduced refrigerant flammability. Int J Refrig 2021;126:133–42. https://doi.org/10.1016/j.ijrefrig.2021.01.003.
[67] B.-M. Lee, H.-H. Gook, S.-B. Lee, Y.-W. Lee, D.-H. Park, N.-H. Kim, Condensation heat transfer and pressure drop of low GWP R-404A alternative refrigerants (R-448A, R-449A, R-455A, R-454C) in a 5.6 mm inner diameter horizontal smooth tube, Int. J. Refrig. 128 (2021) 71-82. 10.1016/j.ijrefrig.2020.12.025.
[68] Schulze C, Raabe G, Tegethoff WJ, Koehler J. Transient evaluation of a city bus air conditioning system with R-445A as drop-in – From the molecules to the system. Int J Therm Sci 2015;96:355–61. https://doi.org/10.1016/j.ijthermalsci.2015.01.033.
[69] Devecioğlu AG, Oruç V. An analysis on the comparison of low-GWP refrigerants to alternatively use in mobile air-conditioning systems. Therm Sci Eng Prog 2017;1:1–5. https://doi.org/10.1016/j.tsep.2017.02.002.
[70] Li G, Eisele M, Lee H, Hwang Y, Radermacher R. Experimental investigation of energy and exergy performance of secondary loop automotive air-conditioning systems using low-GWP (global warming potential) refrigerants. Energy 2014;68:819–31. https://doi.org/10.1016/j.energy.2014.01.018.
[71] M. Xue, N. Kojima, L. Zhou, T. Machimura, A. Tokai, Dynamic analysis of global warming impact of the household refrigerator sector in Japan from 1952 to 2030, J. Clean. Prod. 145 (2017) 172–179. 10.1016/j.jclepro.2017.01.059.
[72] Sethi A, Pottker G, Motta SY. Experimental evaluation and field trial of low global warming potential R404A replacements for commercial refrigeration. Sci Tech Built Environ 2016;22:1175–84. https://doi.org/10.1080/23744731.2016.1209032.
[73] Eyerer S, Wieland C, Vandersickel A, Spliethoff H. Experimental study of an ORC (Organic Rankine Cycle) and analysis of R1233zd-E as a drop-in replacement for R245fa for low temperature heat utilization. Energy 2016;103:660–71. https://doi.org/10.1016/j.energy.2016.03.034.
[74] Yang J, Sun Z, Yu B, Chen J. Experimental comparison and optimization guidance of R1233zd(E) as a drop-in replacement to R245fa for organic Rankine cycle application. Appl Therm Eng 2018;141:10–9. https://doi.org/10.1016/j.applthermaleng.2018.05.105.
[75] Molés F, Navarro-Esbrí J, Peris B, Mota-Babiloni A, Mateu-Royo C. R1234yf and R1234ze as alternatives to R134a in Organic Rankine Cycles for low temperature heat sources. Energy Procedia 2017;142:1192–8. https://doi.org/10.1016/j.egypro.2017.12.380.
[76] Yang J, Ye Z, Yu B, Ouyang H, Chen J. Simultaneous experimental comparison of low-GWP refrigerants as drop-in replacements to R245fa for Organic Rankine cycle application: R1234ze(Z), R1233zd(E), and R1336mzz(E). Energy 2019;173:721–31. https://doi.org/10.1016/j.energy.2019.02.054.
[77] Longo GA, Mancin S, Righetti G, Zilio C, Brown JS. Assessment of the low-GWP refrigerants R600a, R1234ze(Z) and R1233zd(E) for heat pump and organic Rankine cycle applications. Appl Therm Eng 2020;167:114804. https://doi.org/10.1016/j.applthermaleng.2019.114804.
[78] Bianchi M, Branchini L, De Pascale A, Melino F, Ottaviano S, Peretto A, et al. Replacement of R134a with low-GWP fluids in a kW-size reciprocating piston expander: Performance prediction and design optimization. Energy 2020;206:118174. https://doi.org/10.1016/j.energy.2020.118174.

[79] Devecioğlu AG, Oruç V. Characteristics of Some New Generation Refrigerants with Low GWP. Energy Procedia 2015;75:1452–7. https://doi.org/10.1016/j.egypro.2015.07.258.
[80] Park B-S, Usman M, Imran M, Pesyridis A. Review of Organic Rankine Cycle experimental data trends. Energy Convers Manag 2018;173:679–91. https://doi.org/10.1016/j.enconman.2018.07.097.
[81] Dubberke FH, Linnemann M, Abbas WK, Baumhögger E, Priebe K-P, Roedder M, et al. Experimental setup of a cascaded two-stage organic Rankine cycle. Appl Therm Eng 2018;131:958–64. https://doi.org/10.1016/j.applthermaleng.2017.11.137.
[82] STEAG Energy Services GmbH: EBSILON Professional, URL: http://www.steag-systemtechnologies.com/ebsi-lon_professional.html, assessed on 16.05.2021.
[83] Lemmon EW, Huber ML, McLinden MO. Reference fluid thermodynamic and transport properties (REFPROP), version 10.0, in NIST Standard Reference Database 23. Gaithersburg, MD: National Institute of Standard and Technology; 2007.
[84] Uusitalo A, Honkatukia J, Turunen-Saaresti T, Grönman A. Thermodynamic evaluation on the effect of working fluid type and fluids critical properties on design and performance of Organic Rankine Cycles. J Clean Prod 2018;188:253–63. https://doi.org/10.1016/j.jclepro.2018.03.228.
[85] Zhou Y, Liu J, Penoncello SG, Lemmon EW. An equation of state for the thermodynamic properties of cyclohexane. J Phys Chem Ref Data 2014;43:043105. https://doi.org/10.1063/1.4900538.
[86] Gedanitz H, Davila MJ, Lemmon EW. Speed of sound measurements and a fundamental equation of state for cyclopentane. J Chem Eng Data 2015;60:1331–7. https://doi.org/10.1021/je5010164.
[87] Mondéjar ME, Mclinden MO, Lemmon EW. Thermodynamic properties of trans-1-chloro-3,3,3-trifluoropropene (R1233zd(E)): vapor pressure, (p, ρ, T) behavior, and speed of sound measurements, and equation of state. J Chem Eng Data 2015;60:2477–89. https://doi.org/10.1021/acs.jced.5b00348.
[88] Bücker D, Wagner W. Reference equations of state for the thermodynamic properties of fluid phase n-butane and isobutane. J Phys Chem Ref Data 2006;35:929–1019. https://doi.org/10.1063/1.1901687.
[89] Akasaka R, Lemmon EW. Fundamental equations of state for cis-1,3,3,3-tetrafluoropropene [R-1234ze(Z)] and 3,3,3-trifluoropropene (R-1243zf). J Chem Eng Data 2019;64:4679–91. https://doi.org/10.1021/acs.jced.9b00007.
[90] Wu J, Zhou Y, Lemmon EW. An equation of state for the thermodynamic properties of dimethyl ether. J Phys Chem Ref Data 2011;40:023104. https://doi.org/10.1063/1.3582533.
[91] Outcalt SL, McLinden MO. A modified Benedict-Webb-Rubin equation of state for the thermodynamic properties of R152a (1,1-difluoroethane). J Phys Chem Ref Data 1996;25:605–36. https://doi.org/10.1063/1.555979.
[92] Thol M, Lemmon EW. Equation of State for the Thermodynamic Properties of trans-1,3,3,3-Tetrafluoropropene [R-1234ze(E)]. Int J Thermophys 2016;37:28. https://doi.org/10.1007/s10765-016-2040-6.
[93] Qi H, Fang D, Gao K, Meng X, Wu J. Compressed liquid densities and Helmholtz energy equation of state for fluoroethane (R161). Int J Thermophys 2016;37:37–55. https://doi.org/10.1007/s10765-016-2061-1.
[94] Lemmon EW, McLinden MO, Wagner W. Thermodynamic properties of propane. III. A reference equation of state for temperatures from the melting line to 650 K and pressures up to 1000 Mpa. J Chem Eng Data 2009;54:3141–80. https://doi.org/10.1021/je900217v.
[95] Richter M, McLinden MO, Lemmon EW. Thermodynamic properties of 2,3,3,3-tetrafluoroprop-1-ene (R1234yf): Vapor pressure and p – ρ – T Measurements and an Equation of State. J Chem Eng Data 2011;56:3254–64. https://doi.org/10.1021/je200369m.
[96] S. Solmon, D. Qin, M. Manning, M. Marquis, M.M.B Tiguor, H.L. Miller, Z. Chen, Climate Change 2007: The Physical Science Basis. Contribution of Working Group I to the Fourth Assessment Report of the Intergovernmental Panel on Climate Change, Cambridge University Press, Cambridge, United Kingdom and New York, NY, USA, p 996.
[97] J.M. Calm, G.C. Hourahan, Physical, safety, and environmental data for current and alternative refrigerants, Proceedings of the 23rd IIR International Congress of Refrigeration: Prague, Czech Republic, August 21-26, 2011.
[98] Abbas WKA, Linnemann M, Baumhögger E, Vrabec J. Experimental study of two cascaded organic Rankine cycles with varying working fluids. Energy Convers Manag 2021;230:113818. https://doi.org/10.1016/j.enconman.2020.113818.
[99] Safarian S, Aramoun F. Energy and exergy assessments of modified Organic Rankine Cycles (ORCs). Energy Rep 2015;1:1–7. https://doi.org/10.1016/j.egyr.2014.10.003.
[100] Liu W, Meinel D, Wieland C, Spliethoff H. Investigation of hydro fluoroolefins as potential working fluids in organic Rankine cycle for geothermal power generation. Energy 2014;67:106–16. https://doi.org/10.1016/j.energy.2013.11.081.
[101] Giuffrida A. A theoretical study on the performance of a scroll expander in an organic Rankine cycle with hydrofluoroolefins (HFOs) in place of R245fa. Energy 2018;161:1172–80. https://doi.org/10.1016/j.energy.2018.07.146.
[102] Ciconkov R. Refrigerants: There is still no vision for sustainable solutions. Int J Refrig 2018;86:441–8. https://doi.org/10.1016/j.ijrefrig.2017.12.006.